Deformation Behavior of Poly(ether ester) Copolymer As Revealed by Small- and Wide-Angle Scattering of X-ray Radiation from Synchrotron

ARTICLE *in* MACROMOLECULES · MARCH 1997

Impact Factor: 5.8 · DOI: 10.1021/ma9612079 · Source: OAI

7 AUTHORS, INCLUDING:

Zlatan Zlatev Denchev
University of Minho
109 PUBLICATIONS **1,114** CITATIONS
SEE PROFILE

Anton Apostolov
Sophia University
54 PUBLICATIONS **1,027** CITATIONS
SEE PROFILE

Stoyko Fakirov
University of Auckland
240 PUBLICATIONS **3,101** CITATIONS
SEE PROFILE

Deformation Behavior of Poly(ether ester) Copolymer As Revealed by Small- and Wide-Angle Scattering of X-ray Radiation from Synchrotron

N. Stribeck,[†] D. Sapoundjieva,[‡] Z. Denchev,[‡] A. A. Apostolov,[‡] H. G. Zachmann,[†] M. Stamm,[§] and S. Fakirov[‡]

Institut für Technische und Makromolekulare Chemie, Universität Hamburg, 20146 Hamburg, Germany, Laboratory on Structure and Properties of Polymers, 1126 Sofia, Bulgaria, and Max-Planck-Institut für Polymerforschung, Postfach 3148, 55021 Mainz, Germany

Received August 12, 1996; Revised Manuscript Received December 2, 1996[⊗]

ABSTRACT: The deformation behavior of poly(ether ester) is studied by means of small- and wide-angle X-ray scattering (SAXS and WAXS). The material under investigation represents a polyblock thermoplastic elastomer of poly(ether ester) (PEE) type. It comprises poly(butylene terephthalate) (PBT) as hard segments and polyethylene glycol (PEG) as soft segments in a ratio of **57/43** wt %. Isotropic PEE bristles are drawn to five times of their initial length and subsequently annealed with fixed ends for 6 h at 170 °C in vacuum. The WAXS patterns were registered by a pinhole camera and a 2D area gas detector. These measurements were performed both under stress and during the subsequent relaxation in the absence of stress. The deformation was increased stepwise up to the breaking point of the sample (ca. 185%). SAXS patterns were obtained in the same deformation range by means of monochromatic X-ray radiation in the beamline A2 of the synchrotron DESY in Hamburg, Germany. SAXS patterns were registered by means of a 2D "Image-plate" detector. Five deformation intervals were revealed by SAXS. In the first one ($\epsilon = 0-50\%$) an ensemble of uncorrelated strained microfibrils exists and the corresponding layer line small-angle pattern is observed. These microfibrils scatter independently. In the second interval ($\epsilon = 50-80\%$) interactions between neighboring microfibrils develop, a microfibrillar network is observed, and the layer line pattern transforms into a four-point diagram. In the third interval ($\epsilon = 80-100\%$) two additional reflections show up and an unique six-point pattern is seen. Pull-out of tie molecules from crystallites begins to fibrillate the network. This pull-out mechanism is independently proved by WAXS. In the fourth interval ($\epsilon = 100-130\%$) the mean long period of the four-point pattern decreases and the pattern itself vanishes. At last the fiber is completely fibrillated and only a two-point pattern remains visible. In the second, third, and fourth intervals, the microfibrils correlate in the transverse direction, which allows determination of the interfibrillar distance (so-called transverse long period). It decreases gradually with the progress of deformation in both the strained and relaxed state. In the fifth interval ($\epsilon > 130\%$) the long period of the two point pattern remains constant, but its intensity decreases until the fiber breaks. Only a few microfibrils are simultaneously carrying the load. They are destroyed one by one, until the fiber breaks as a whole.

Introduction

Thermoplastic elastomers represent a relatively new class of engineering plastics and are distinguished by some peculiarities that make them a very interesting subject of research.[1] Among the big variety of thermoplastic elastomers synthesized and studied so far, those based on segmented polyblock poly(ether esters) have attracted special attention. They comprise repeating, high-melting, crystallizable blocks (hard segments) and noncrystallizable blocks having a relatively low glass transition temperature (soft segments). Typically the hard segments are composed of multiple short chain ester units [usually tetramethylene terephthalate, commonly called poly(butylene terephthalate) (PBT)], whereas the soft segments are derived from aliphatic polyether or polyester glycols.[2]

At useful service temperatures, the thermoplastic elastomers resist plastic deformation since they feature a network of chain molecules interconnected by microcrystallites. This network is formed as a result of partial crystallization of the hard segments, the microcrystallites functioning as physical cross-links. At processing temperatures, these crystallites melt to yield a polymer melt which after shaping, e.g., by molding, retains its form upon cooling due to recrystallization of the hard segments.[2]

A big variety of starting materials can be used for preparation of segmented polyblock elastomers. By varying the ratio of hard to soft segments, materials ranging from soft elastomers to relatively hard plastics can be obtained. To develop a better understanding of the material properties it is thus necessary to accumulate elementary data on the properties of the crystallizable and noncrystallizable segments. This means to determine the morphology of these polymers under various conditions, including application of stress and different temperature treatment. One of the techniques that proved to be useful to this purpose is the scattering of X-rays in all its variants, namely SAXS or WAXS, performed by means of an X-ray tube or synchrotron radiation. In our early SAXS studies[3] on oriented poly(ether ester) containing PBT as hard segments and poly(ethylene glycol) (PEG) as soft segments, a directly proportional increase of the long spacing with the applied stress was found up to a relative deformation of $\epsilon = 100\%$. At higher deformations pulling out of tight tie molecules from adjacent microfibrils occurs and some of the microfibrils relax. Two long periods coexist for some deformations. A model was suggested that adequately described the behavior of the polymer system under and without application of stress.[3]

[†] Universität Hamburg.
[‡] Laboratory on Structure and Properties of Polymers.
[§] Max-Planck-Institut für Polymerforschung.
[⊗] Abstract published in *Advance ACS Abstracts,* February 1, 1997.

S0024-9297(96)01207-7 CCC: $14.00

In subsequent investigations, the same approach and model were successfully applied to characterize the changes in the SAXS patterns of a set of six PBT/PEG poly(ether ester) segmented block copolymers varying in their hard-to-soft segment ratio.[4] In the same work a way for estimation of the fractions of both intra- and interfibrillar amorphous material was suggested. A usual small-angle (Kratky) camera was employed in this study.

By means of a two-dimensional detector it was possible to further develop the model, revealing finer details in the copolymer structure.[5] So at low macrodeformations two-point SAXS patterns of the oriented PBT/PEG segmented block copolymer were obtained. It was accepted that the sample morphology represents assemblies of parallel crystalline lamellae positioned perpendicularly to the stretching direction. In the unloaded, relaxed state, the observed four-point patterns were explained by a zigzag arrangement of lamellae, the crystalline layers being inclined to the stretching direction. The observed morphological transition was found to be reversible and revealed more and more as the final deformation in the cycle was increased. A well-pronounced dependence of the SAXS characteristics on the molecular weight of the sample was also pointed out.

Our recent SAXS study on a thermoplastic elastomer based on PBT and PEG demonstrated the occurrence of a more complicated, "six-point" SAXS pattern in both stressed and relaxed oriented bristles.[6] Such a diffraction pattern indicates a coexistence of two basic morphological ensembles. For some technical reasons these results were impossible to reproduce in later investigations of the same sample; only two- and four-point diagrams were observed. However, applying computerized graphical analysis of the patterns, we managed to demonstrate their complex character and obtained evidence, although indirect, of a six-point diagram.[7]

All SAXS studies mentioned above were performed using conventional, relatively low-power X-ray sources from a simple or a rotating anode tube. For this reason we looked for a more powerful source, such as synchrotron radiation which offers basically new opportunities for morphological investigations.

The goals of this study are (i) to try to reveal a six-point SAXS diagram from the same thermoplastic elastomer employing the more powerful synchrotron radiation, (ii) to improve the model ideas about deformation and relaxation processes and in particular the pull-out mechanism suggested previously,[3] and (iii) to approach a real-time investigation of the deformation and relaxation processes by drastically decreasing the exposure time from several hours to 2 min.

Experimental Section

Sample Preparation and Pretreatment. The material under investigation represents a thermoplastic elastomer of polyblock poly(ether ester) (PEE) type. It comprises poly(butylene terephthalate) as hard segments and polyethylene glycol (PEG) as soft segments. The latter have an average molecular weight of 1000 and polydispersity of 1.3, as found by means of gel permeation chromatography.[3] Such PEE with a hard-to-soft segment ratio of 57/43 wt % was prepared by polycondensation on a semicommercial scale in a manner well-known and described elsewhere.[8] A stabilizer based on a phenolstyrene antioxidant (BFSA) was added to the as-prepared molten material to achieve maximum durability and superior mechanical properties.[8] The melt was then pressed through a die and the isotropic bristles thus obtained were drawn at room temperature to five times their initial length. The samples for the X-ray scattering measurements were produced by subsequent annealing with fixed ends of the stretched bristles for 6 h at 170 °C in vacuum.

Wide-Angle X-ray Measurements. The wide-angle X-ray scattering (WAXS) of the samples was measured by a pinhole camera on an 18 kW rotating-anode tube using Cu Kα radiation and a graphite double monochromator. An area gas detector with 512 × 512 pixels was used with the sample-to-detector distance set at 6.8 cm. Measurements under stress were performed using a frame allowing controlled variation of the sample length. Each measurement under stress was followed by one in the absence of stress (in the "relaxed state") before a larger deformation was applied in the subsequent cycle. The exposure time ranged between 2 and 15 h. Thus the samples were studied in the 0−185% deformation range by measurements at $\epsilon = 0$, 20, 50, 75, 100, 125, 150, and 185% relative deformation. Here and in the following, ϵ is defined as

$$\epsilon = 100\,\frac{l - l_0}{l_0} \tag{1}$$

where l_0 and l are the initial and the actual bristle length, respectively, as measured between two marks close to the irradiated center of the bristle. In the case of the measurements in the relaxed state, the same equation was used to compute the residual deformation ϵ_r, where l_0 is again the initial length of the predrawn sample.

In addition to the patterns from sample under stress, seven more patterns were obtained from the relaxed samples. They are denoted as 4.5(20), 11(50), 24(75), 34(100), 50(125), 80(150), and 95(185). Here the first number represents the residual (plastic) deformation percentage after an elongation given by the number in parentheses.

All two dimensions (2D) WAXS patterns were obtained and processed by means of the General Area Detector Diffraction Software from Siemens. For each diffraction pattern displayed in this paper, the corresponding fiber was orientated vertically.

To reduce the statistical noise, the patterns were averaged over four pixels in a square. Equatorial sections were then made for every deformation. In all sections the intensity was averaged again over five pixels in the vertical direction. The data were corrected for background scattering, detector efficiency, counting time, and the change of sample volume during stretching. This made all sections comparable with one another.

Small-Angle X-ray Scattering Measurements. Small-angle X-ray scattering (SAXS) patterns were obtained using the same samples and deformation range. Synchrotron radiation generated at the beamline A2 of the synchrotron in Hamburg, Germany, was applied. The sample-to-detector distance was set to 2075 mm. Diffraction patterns were registered by means of a 2D image-plate detector. The exposure time was 2 min. An area of 900 × 900 pixels, each with a size of 176 μm × 176 μm, was read out and used for the evaluation. After each exposure under stress the sample was released while the detector plate was exchanged within 1 min. After that another exposure was carried out, while the macroscopic shrinking process of the sample was still going on. Within the following minute the image plate was exchanged and the sample was drawn to reach the subsequent elongational step in the series. Immediately after that a new cycle started. Thus, as a function of an increasing final deformation, 16 patterns under stress and 15 patterns during relaxation were recorded.

SAXS Data Processing. A typical SAXS diffraction pattern obtained under the above conditions at $\epsilon = 88\%$ is displayed sketchily in Figure 1. The isolines denote equal intensity. The vertical direction coincides with fiber axis (FA) and stretching direction (SD). The lines indicate how and where sections and projections of the intensity are made. The wave vector components in horizontal and vertical direction are denoted as s_{12} and s_{13}, respectively. The horizontal line $a-a$ shows the direction of a horizontal (off-equatorial) section. Central vertical (meridional) sections were extracted through the center of the pattern (line $b-b$) and the overall intensity in the pattern was projected on to the same using the equation

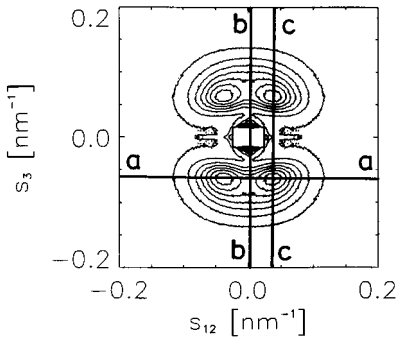

Figure 1. Sketch of the 2D diffraction pattern for $\epsilon = 88\%$. The stretching direction (SD) is vertical. The wavevector components in the horizontal and vertical directions (s_{12} and s_3, respectively) are shown. The lines indicate how and where sections and projections of the intensity are made (see the text).

$$I_\rho(s_3) = \int_0^\infty s_{12} I(s_{12},s_3)\, ds_{12} \qquad (2)$$

where $I(s_{12},s_3)$ is the corrected scattered intensity. Due to the cylindrical symmetry of all the SAXS patterns $I_\rho(s_3)$ represents a one-dimensional scattering curve characterizing the changes of the electron density ρ in one direction only. By projecting the intensity in the pattern on the direction parallel to the fiber axis, this direction was chosen to be the FA. An off-meridional section was made through the maxima as indicated (line $c-c$).

The intensity decay of the incident primary beam was monitored by an ionization chamber and the intensity in the pattern corrected accordingly. Additional intensity correction was made to compensate for the changes in the irradiated volume during the stretching. Due to the primary beam geometry, only the diameter of the sample changes with the deformation, while the irradiated length remains constant. In order not to damage the sample during the scattering experiment, the diameter of the fiber was measured in a separate straining experiment for several deformations using a micrometer screw, and a smooth correction curve was obtained by interpolation between these data points. This experimental correction turned out to be more appropriate than the one deduced theoretically under the assumption of an entirely entropic deformation process. This is also proved by the existence of residual (plastic) deformation.

In Figure 2 selected sections and a projection of the scattered intensity onto SD (vertical) are shown. I_ρ denotes projection whereas I denotes section. The off-meridional section through the maxima of a four-point pattern reveals a well-expressed maximum. A complete data evaluation of the projections in terms of a one-dimensional structural model is planned in the future. Here one can already observe that the (weighted) addition of as many as 200 sections in every projection improves the signal-to-noise ratio and thus the data reliability.

Results

Dependence of the Long Spacing L on the External Deformation As Revealed by SAXS. As already mentioned, the main task of this investigation was to reproduce measurements, by means of synchrotron radiation, which already had been performed previously using a rotating anode tube[3,9] and thus to enhance the quality of the recorded data. The effect of the external deformation ϵ on such an important structural parameter as the long spacing L, as well as on the morphology of PEE, was followed in ref 3. The previous paper reports *steady state* measurements, i.e., an equilibrium state of the sample was achieved before taking the diffraction pattern and this state remained constant while data was recorded.

Because of the high primary beam intensity of the synchrotron radiation device, it was possible to reduce the recording time to 2 min. In this way we hoped to obtain more information on the deformation and subsequent relaxation processes taking place in the relatively new type of thermoplastic elastomers. Moreover, we used a new sample, characterized by the same chemical composition but possessing very high drawability (1300%[8] vs 800% for the sample, used earlier[10]) due to the use of a new antioxidant.[8] It was interesting to compare how this high drawability corresponds to the deformation ability.

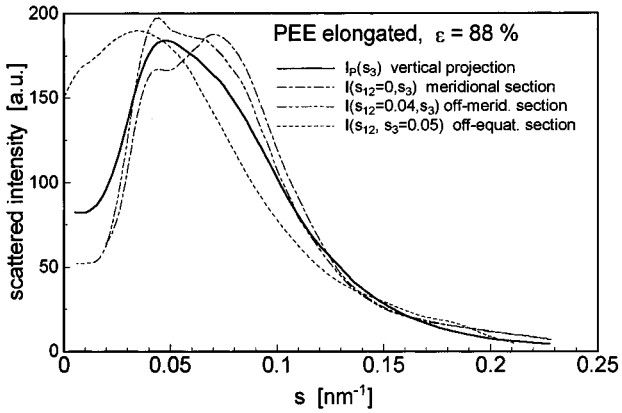

Figure 2. Selected sections and projection of the scattered intensity onto SD.

In Figure 3 selected 2D SAXS patterns under stress (a) and in the relaxed state (b) are shown. To present the patterns, a color-lookup table (rainbow) is used repeatedly so that both the shape and intensity variations of the patterns can be visualized appropriately. In Figure 3a the parameter below each pattern denotes the overall (external) deformation in percent, whereas in Figure 3b it denotes the residual deformation. The number in parentheses in the second case is the preceding overall deformation under stress in percent. A two-point pattern can be observed for the initial (unstrained) sample. Up to a deformation of 48%, the observed pattern does not change its shape in both the stressed and the relaxed state, but turns into a four-point one for the next two deformations of 68 and 80% in both states. A unique six-point pattern appears for the following three deformations of 88, 98 and 110%, the corresponding patterns in the relaxed state being the four-point type. This six-point pattern can be considered as a superposition of a two- and a four-point pattern. For higher deformations, the two-point pattern takes over and is solitarily observed up to the break of the sample at ca. 200%. Within the same deformation range in the relaxed state, the four-point pattern gradually transits into a two-point one.

From the 2D patterns as shown in Figure 3, off-equatorial sections through the maxima were extracted (cf. Figure 1, $a-a$). Similarly, off-meridional sections through the maxima (Figure 1, $c-c$) and meridional sections (Figure 1, $b-b$) as well as projections onto SD were obtained (cf. Figure 2). Hence, some important parameters were computed from the positions of the maximum intensity in the sections, namely the long spacing L in the direction of stretching (also called longitudinal long spacing, or shortly long spacing) and the long spacing in the transverse direction L_{hor}, i.e., the distance between the microfibrils, measured on a horizontal line.

Figure 4 shows the dependence of the long spacing L on the overall deformation ϵ in both the strained and the relaxed state. In the strained state the initial long spacing L_0 increases linearly with the deformation up to a value of $\epsilon = 80\%$ (Figure 4, see L_1) and then steeply

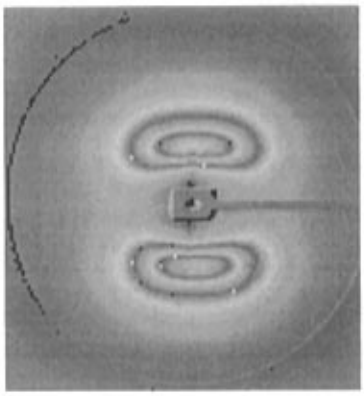

ε = 0 %

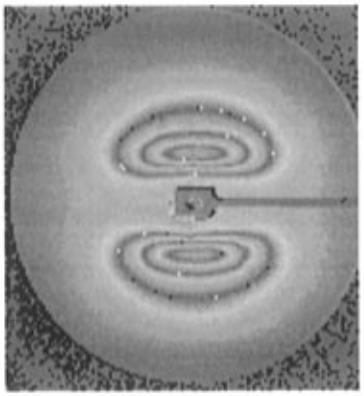

ε = 34 %

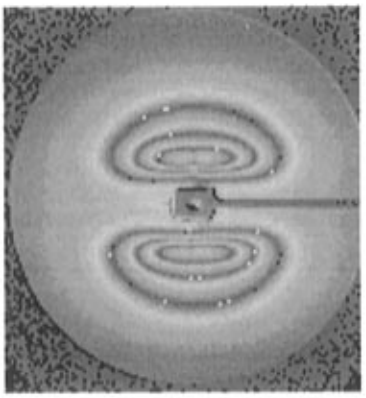

ε = 48 %

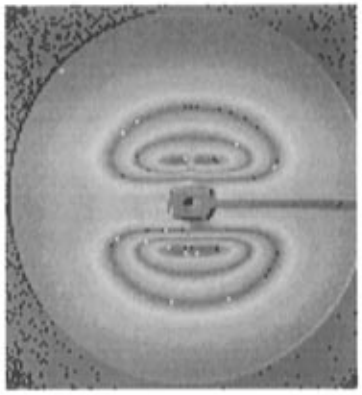

ε = 60 %

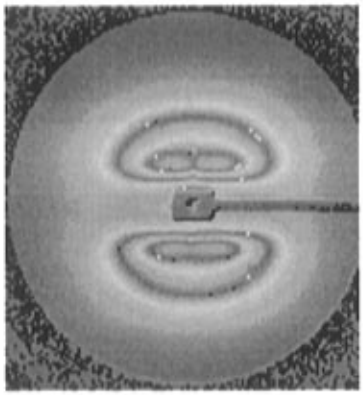

ε = 68 %

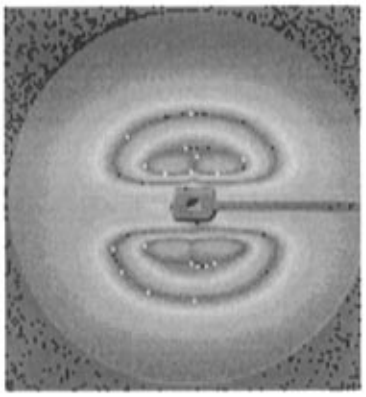

ε = 80 %

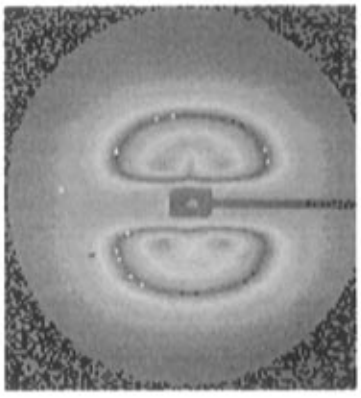

ε = 88 %

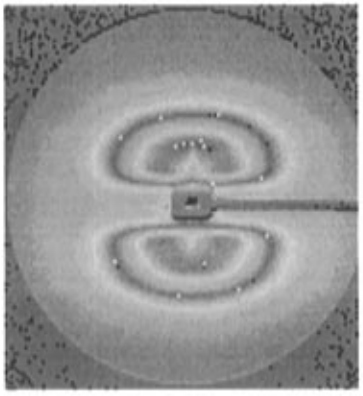

ε = 98 %

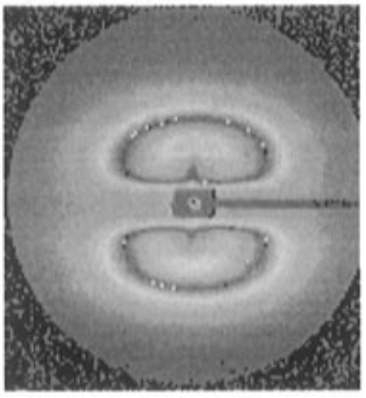

ε = 110 %

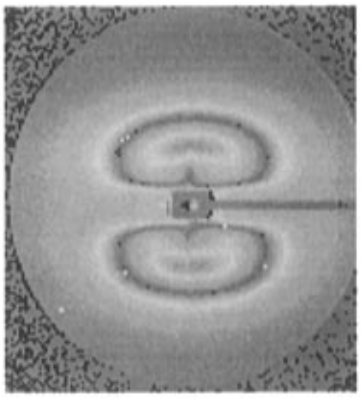

ε = 128 %

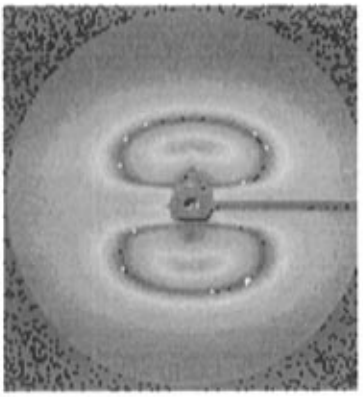

ε = 134 %

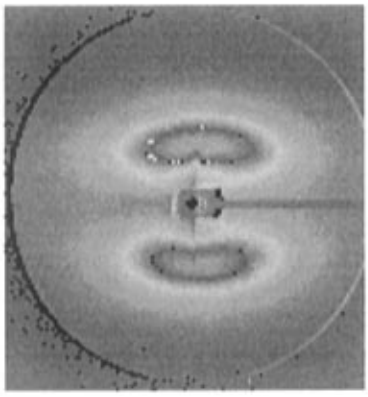

ε = 184 %

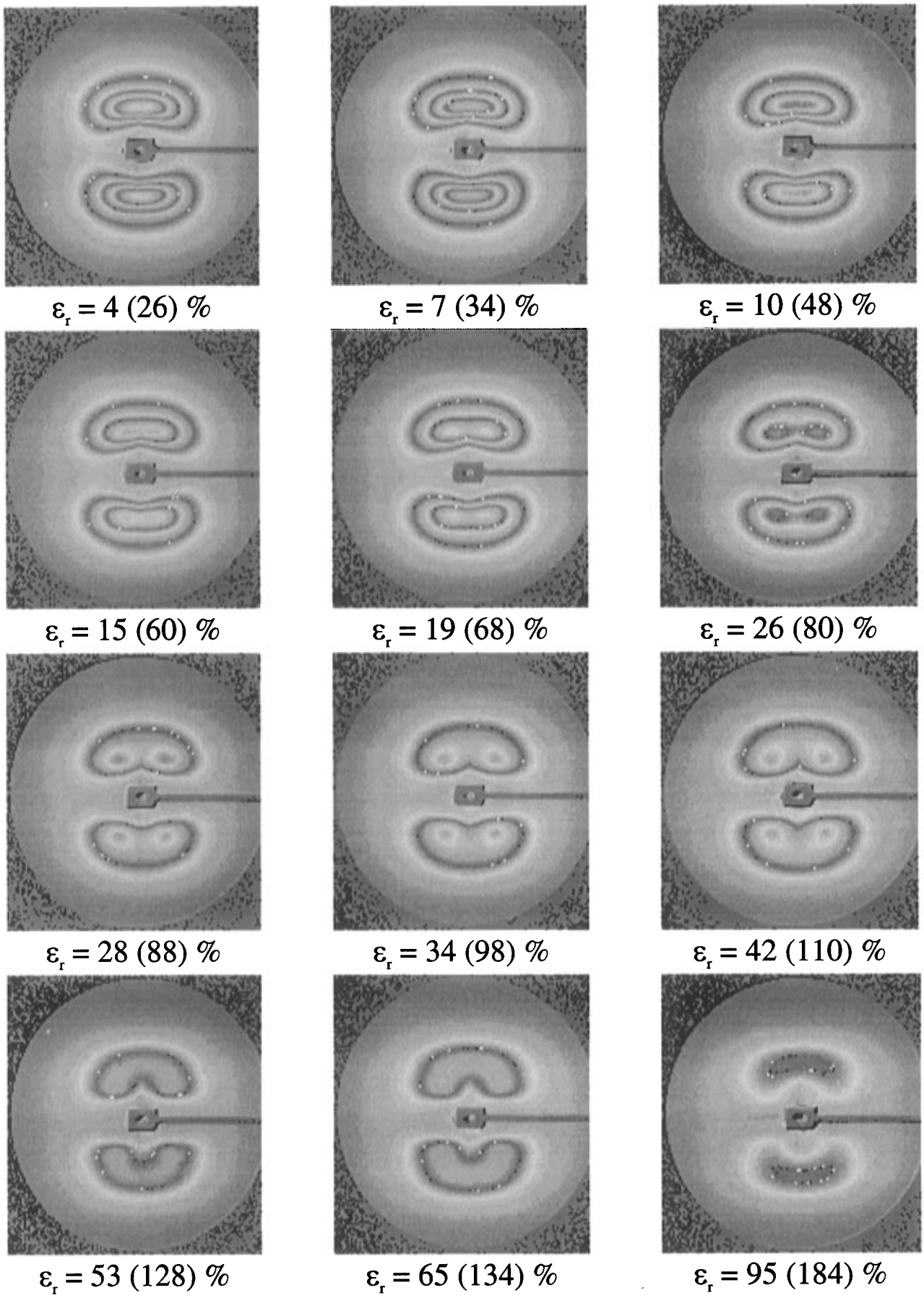

Figure 3. Selected 2D SAXS patterns as follows: (a, left page) in the elongated state at the marked overall deformation ϵ, (b, right page) in the relaxed state at the marked residual deformation ϵ_r after applying the overall deformation in parentheses. Stretching direction vertical.

decreases down to L_2, which is very close to its initial value, in agreement with earlier results on the same sample.[3] In the intermediate region of ϵ between 80 and 128%, two long spacings can be seen, differing by 5−6 nm. They merge for deformations of 134% and higher. In the relaxed state, the long spacing for lower deforma-

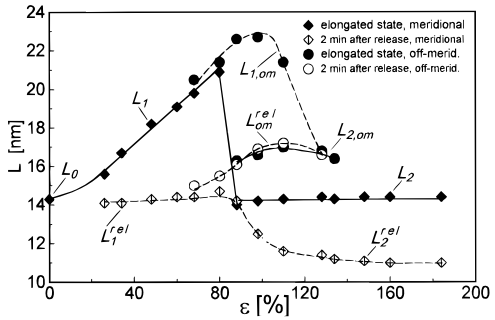

Figure 4. Dependence of the longitudinal long spacing (L) on the deformation (ϵ) for sample in elongated and relaxed state.

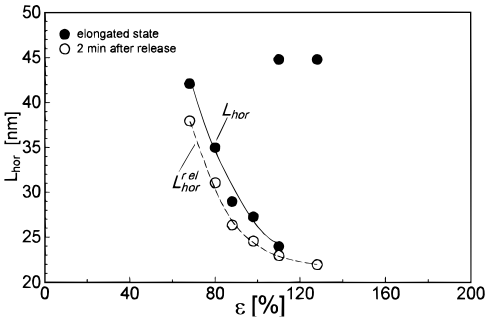

Figure 5. Dependence of the transverse long spacing (L_{hor}) on the deformation (ϵ) for sample in elongated and relaxed state.

tions, L_1^{rel}, remains constant up to the intermediate deformation range and then decreases steadily for higher deformation down to a value of $L_2^{rel} = 11$ nm, which is 3 nm lower than the initial value L_0. The recovering of the initial value of L after the removal of stress points out that its rise under stress is due to conformational changes in the amorphous regions only; i.e., the external stress results in stretching of the chains in the amorphous interlamellar regions. After the removal of the external stress, these chains relax toward their initial state, thus recovering the initial value of L_0.

As already mentioned, L is proportional to ϵ up to $\epsilon = 80\%$ and then drops to its initial value and remains constant with the further rise of ϵ. In agreement with previous results,[3,9] such an abrupt decrease of L_1 can be explained by a drastic decrease of the number of interfibrillar contacts due to pulling out tight interfibrillar tie molecules from the hard domains at intermediate deformations (a process which, as well, damages the involved hard domains). At a deformation of ca. 80% a second long spacing, L_2, appears, which can be explained by the relaxation of a fraction of the microfibrils after their interfibrillar contacts have been destroyed.

After the external stress is removed, one now observes a long spacing L_2^{rel} lower than L_0. This observation can be explained in continuation of the notion already developed: Since in the remaining microfibrils of the ensemble the restriction by the interfibrillar bonds has dropped, relatively more microfibrils than in the initial sample are able to relax completely and the average long spacing is reduced. These changes of the long period have already been observed earlier.[3,9] In the present work, though, the measuring time was only 2 min, in contrast to 2−15 h in the previous studies.[3,9]

Of particular importance are the results for the range $\epsilon = 80-110\%$, where during the transit from the two-point to a four-point pattern an intermediate six-point pattern is exhibited. Hence, starting from here additionally off-meridional sections through the two off-meridional maxima were evaluated (Figure 1, $c-c$) and numerical values for long spacing of the off-meridional component were determined. As a peculiarity, these sections for one and the same deformation show two peaks (cf. Figure 2) corresponding to two long spacings (see Figure 4, $L_{1,om}$ and $L_{2,om}$). The common meridional sections from the stressed state yield the long spacings, L_2, which originate from the coexisting two-point pattern.

Moreover, the off-meridional long spacing in the relaxed state L_{om}^{rel} is equal to one of the two off-meridional long spacings observed under stress, namely to $L_{2,om}$ (Figure 4). These patterns point to some peculiar structure of the stacks, the morphological features of which will be considered later. It is worth mentioning here that a structure leading to a six-point pattern was suggested earlier by a computerized analysis of scattering curves which had been obtained from a typical four-point pattern recorded by means of a rotating anode X-ray source.[7]

Dependence of the Interfibrillar Distance L_{hor} on the Overall Deformation As Revealed by SAXS. Due to the very high power of the synchrotron radiation source, very smooth and intense scattering patterns may be obtained. This is not always possible with the use of an ordinary X-ray source. It is of particular importance to obtain well-expressed four-point patterns, since a horizontal (off-equatorial) scan (Figure 1, $a-a$) of such a pattern through the maxima can bring into light important information concerning the interfibrillar distance.[11] This parameter, measured in our case in horizontal direction, can be called transverse long spacing and designated as L_{hor} by analogy with the longitudinal long spacing L. It can be derived from a four-point diffraction pattern when the hard domains of the microfibrils arrange in such a way that they form a distorted macrolattice in more than one dimension.[11,12] Since the six-point pattern may be regarded as the superposition of a two- and four-point pattern, it can also be used to calculate L_{hor}. The data derived from the four- and six-point patterns of Figure 3 are shown in Figure 5.

As seen from Figure 5, L_{hor} steadily decreases from 43 nm at $\epsilon = 68\%$ deformation to 24 nm at $\epsilon = 110\%$ for the strained sample. This decrease of the interfibrillar distance by almost a factor of 2 is a result of the longitudinal sample stretching from 68 to 110%. The same dependence for the relaxing sample shows a similar trend, except for the fact that the L_{hor} values are several percent smaller; i.e., the interfibrillar distance practically does not depend on whether or not the sample is in the strained state or in the beginning of the relaxation. It appears that the microfibrils draw closer due to the stretching, which results in the observed decrease of the interfibrillar distance. With progress of deformation, the intensity of the four-point maxima decreases considerably. Bearing in mind the microfibrillar model,[13] this observation can be explained by a pull-out of the interfibrillar tie molecules, a process which destroys a multidimensional (macrolattice) correlation among hard domains of adjacent microfibrils and/or preferentially destroys those hard domains which before had been arranged in such a multidimensional macrolattice. Up to a deformation of $\epsilon = 110\%$, the four-point pattern component has almost vanished while the old two-point maximum has spread and turned into a layer line. This layer line indicates an ensemble of

microfibrils containing hard domains with only a one-dimensional correlation along FA. As the old four-point pattern vanishes at $\epsilon = 110\%$, the layer line itself appears to split about the meridian and thus turns into a four-point pattern itself, indicating the development of multidimensional correlation among the corresponding microfibrils, and the determination of an L_{hor} is desirable. Since the effect is rather weak, the sample thins and thus the noise of the analyzed curves becomes higher, and the reliability of the determination vanishes with increasing elongation. In Figure 5 the two unconnected data points (filled circles) represent the values for the interfibrillar distance of this component for those two steps of deformation where the analysis was still possible.

Dependence of the Crystalline Perfection on the Overall Deformation As Revealed by WAXS. In order to clarify the morphological peculiarities of the sample under and without stress, WAXS patterns were taken for the same sequence of stretching−relaxation cycles. In Figure 6 selected wide-angle 2D-patterns under stress and in the relaxed state are shown. As seen from these patterns, the shape and the size of the reflections both in radial and in the azimuthal direction change with the progress of the overall ϵ and the residual ϵ_r deformation. In order to obtain more precise information, equatorial sections of the 2D-patterns were taken for all deformations. The results are shown in Figure 7 for samples under stress (Figure 7a) and in the relaxed state (Figure 7b). The overall deformation ϵ or the residual deformation ϵ_r, respectively, was taken as a parameter. It is clearly seen that the (010)-reflection and even more the (100)-reflection broaden as a function of deformation for samples under stress. To a minor extent the relaxed samples show the same trend.

It is well-known that the width of the wide-angle reflections is correlated with the imperfection of the crystallites. Decreasing crystallite size and increasing crystallite distortions as well as increasing disorientation of the crystallites broaden the reflection. For this reason the full width at half-height (FWHH) of the reflections, shown in Figure 7, was measured as a function of the deformation. Figure 8 shows the FWHH of both the (010)- and (100)-reflections for the sample under stress vs the overall deformation (Figure 8a) and for the sample in the relaxed state vs the residual deformation (Figure 8b). For the elongated sample (Figure 8a) the FWHH of both the reflections increases as a function of the overall deformation up to $\epsilon = 100\%$ and remains constant for higher deformations within the experimental error. For the relaxed sample (Figure 8b) the FWHH of both the reflections increases as a function of the residual deformation up to $\epsilon_r = 34\%$ and remains constant for higher deformation within the experimental error ($\epsilon_r = 34\%$ corresponds to $\epsilon = 100\%$). As in the case of the SAXS measurement (cf. Figures 4 and 5), a change in the trend of some structural parameter (in this case the width of the reflections) occurs at $\epsilon \approx 100\%$.

Discussion

Some qualitative conclusions concerning the sample morphology can be drawn on the basis of the small-angle 2D patterns (Figure 3). The basic morphological entities of the investigated highly oriented and semicrystalline PEE can be considered as an ensemble of microfibrils, orientated parallel to the fiber axis and consisting of alternating hard regions and soft segment regions. Because of their correlated arrangement along the fiber axis (only one-dimensional) these microfibrils generate the initially observed layer-line pattern. If the microfibrils are closely packed, they can as well be considered as an ensemble of rippled and stacked layers, with wavelengths and amplitudes of the surface undulations being distributed at random within a length-scale interval which is at least of the same order of magnitude as compared to the long spacing.[14] So if we decide to define a layer structure only by the property of connectivity (i.e. lateral extension), we cannot distinguish whether the initial structure is built from layers or from microfibrils. But if we decide that the notion of layers additionally requires the domains to be more or less flat, the initial structure is surely only microfibrillar, since the shape of the initially observed SAXS reflections appears to be considerably extended in equatorial direction. Thus the initial two-phase morphology of the multiblock copolymer lacks the property of flatness.

Following Peterlin[13] one may introduce multidimensional correlation into such an ensemble of microfibrils and thus create a variety of morphologies. If the hard-segment domains of adjacent and densely packed microfibrils tend to arrange in such a way that they form a common and more or less flat surface, one obtains a lamellar system (where the lamellar surface may be tilted or normal to the fiber axis). Would this mechanism occur during deformation, one would either observe an ongoing concentration of the scattered intensity about the meridian (for lamellar surfaces perpendicular to FA) or an ongoing concentration of the scattered intensity about two tilted axes in the pattern (for tilted surface normals). If, on the other hand, the hard-segment domains of neighboring microfibrils either tend to avoid contact or if they do not fill the volume of the sample, multidimensional correlation will yield a short-range correlated "macrolattice".[11] Again, if volume-filling is assumed, such a system may be considered as an ensemble of layer stacks containing "corrugated lamellae", in which the wavelength distribution of the surface undulations shows a pronounced maximum, namely the mean corrugation wavelength. Would this mechanism occur during deformation, one would simply observe the development of a dent in the center of each layer line while the form factor envelope would not change. After a while, one would no longer call the diagram a two-point pattern but name it a four-point pattern.

Although both the tilted lamellae and the microfibrillar macrolattice yield SAXS four-point patterns, one can distinguish them from one another. According to basic considerations of scattering physics (particle and lattice factor),[15,16] which have been verified by model calculations,[17−19] tilted lamellae show the typical "cloverleaf" or "butterfly" shape of the SAXS pattern, which has been observed by several authors.[17,20−22] No indication of such a shape can be observed in any of the newly recorded high-resolution scattering patterns, which means that the microfibrillar model appears to be more adequate for the description of the present structure than the notion of stacks from flat, extended, and tilted lamellae. Nevertheless, the existence of tilted-lamellae stacks even in the elongated state with its well developed four-point patterns cannot be excluded completely, since the expected cloverleaf shape of the particle factor may be hidden behind a faint residue of the two-point diagram observed in the beginning of the straining series.

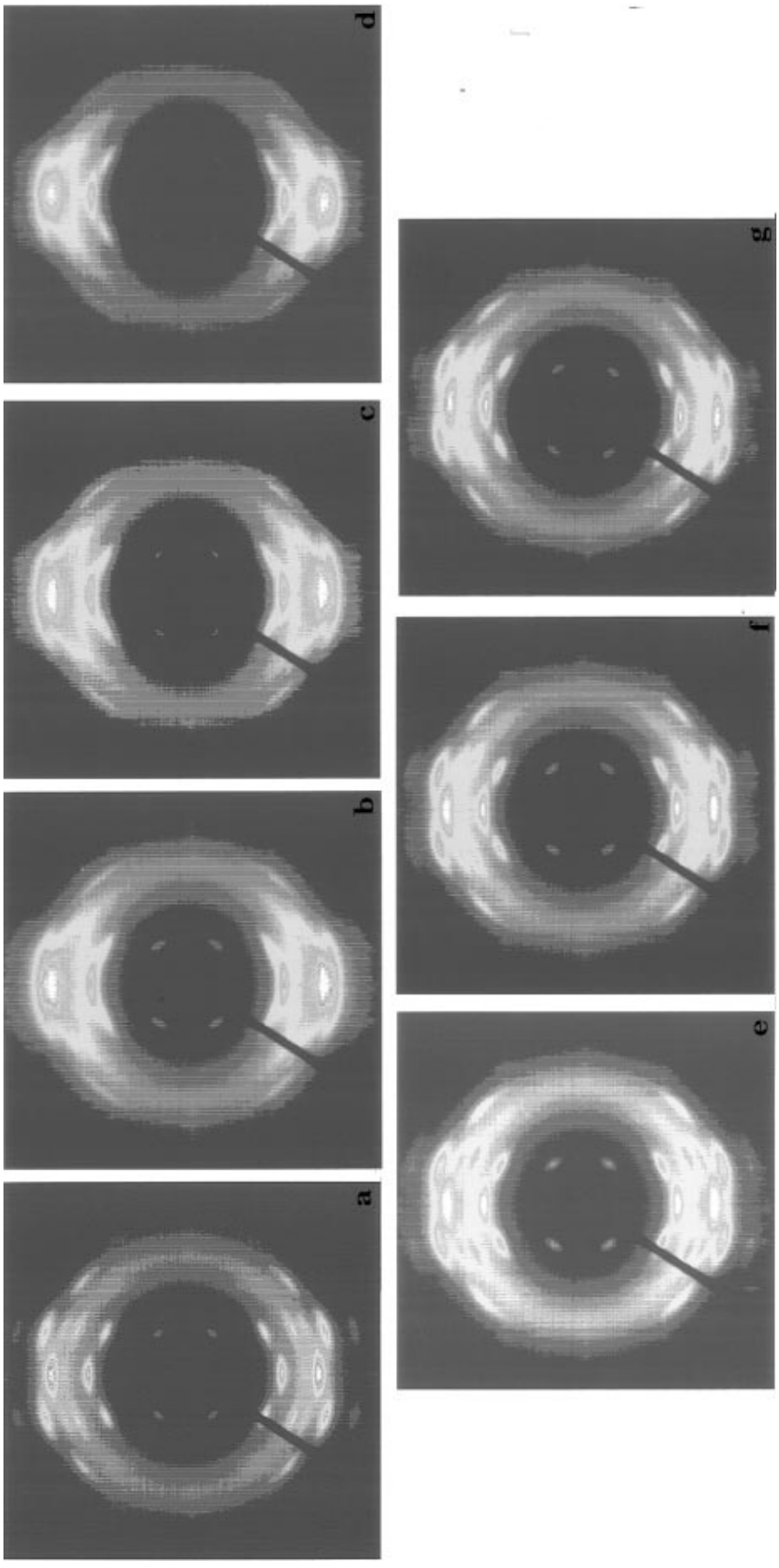

Figure 6. 2D wide-angle patterns of PEE taken under (upper raw) and without (lower raw) stress. The deformation under stress (ϵ) is as follows: (a) 0 (initial sample), (b) 100, (c) 150, (d) 185. The deformation in relaxed sample (ϵ_r) is as follows: (e) 35(100), (f) 80(150), and (g) 95(185). The preceding overall deformation is given in parentheses.

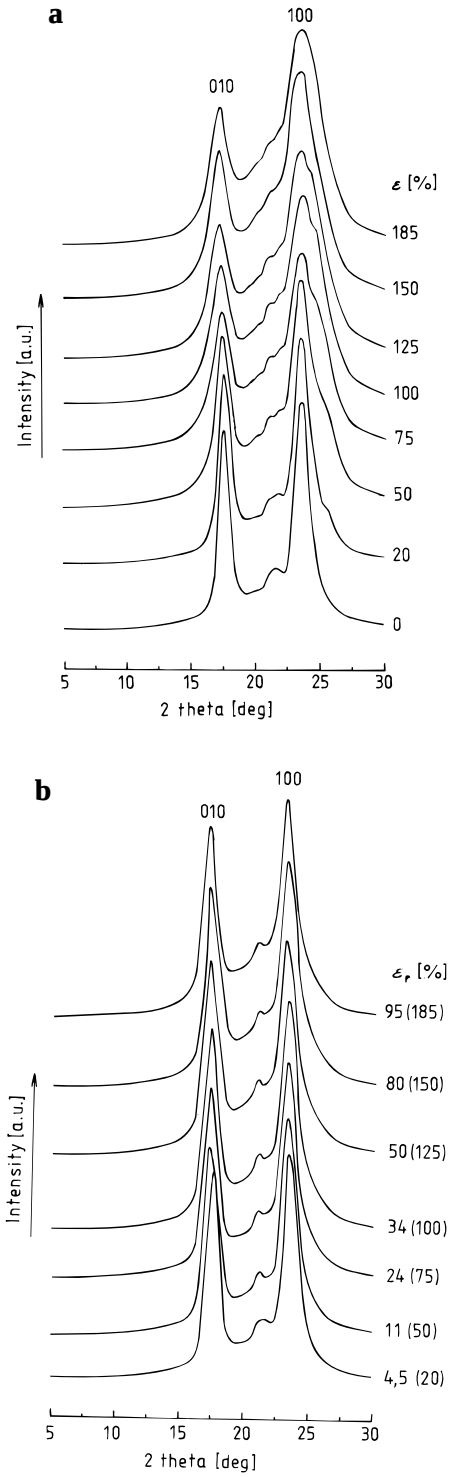

Figure 7. Equatorial sections of 2D wide-angle patterns taken (a) under stress at the indicated overall deformation (ϵ) in percent and (b) taken in the relaxed state at the indicated residual deformation (ϵ_r) in percent. The number in parentheses denotes the preceding deformation. The numbers above the peaks are Miller's indices.

After a thorough study of Figure 3a, five deformation intervals can be distinguished. In the first one (ϵ = 0−48%) the diffraction pattern consists of two layer line reflections which draw closer with the rise of the deformation. The shape of the maxima and their position correspond to microfibrils with relatively narrow diameter (as compared to the observed long period), which are undergoing an elongation. There is no interaction among the different microfibrils in the ensemble.

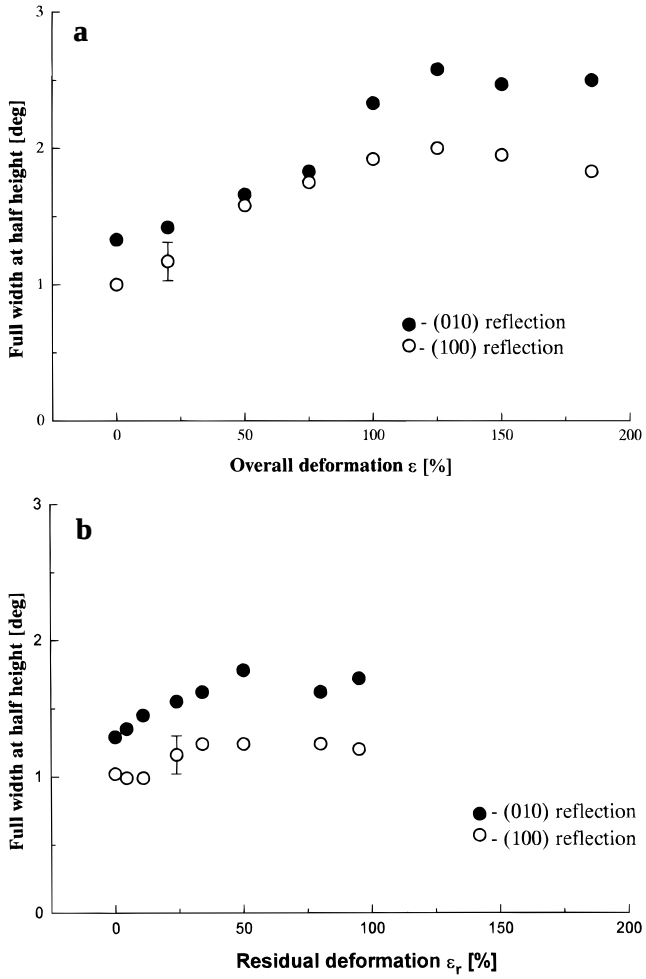

Figure 8. FWHH of (010)- and (100)-reflections of PBT vs (a) the overall deformation (ϵ) and (b) the residual deformation ϵ_r in percent.

For deformations of 48% and larger (Figure3 a), a four-point pattern develops, indicating that neighboring microfibrils begin to arrange their hard domains with respect to each other. This interaction between adjacent microfibrils minimizes the load of taut tie molecules between them. All through the second deformation interval (ϵ = 50−80%) a clearly indicated four-point pattern can be seen, while the elongation within the microfibrils is proceeding.

At ϵ = 88% two additional reflections appear; i.e., a six-point small-angle pattern can be observed throughout the third deformation interval (ϵ = 80−100%). As pull-out of tie molecules occurs and hard domains are destroyed, more and more of the remaining microfibrils relax and, again, show the layer line pattern of uncorrelated fibrils. Although the qualitative trend of the pattern change could as well be explained by a breaking of tie molecules, the quantitative trend is an obvious hint for the pull-out mechanism. A considerable decrease of the scattering power can be estimated, if one compares the patterns, which are calibrated to unit irradiated volume. In order to explain this decrease, one has to assume at least one of two effects, which both favor the pull-out mechanism, namely, a decrease of the contrast between the hard- and the soft-domain phases or a considerable decrease of the volume fraction of hard domains. Only pull-out will destroy hard domains and increase the electron density of the soft phase. The fiber begins to become fibrillated, while the straining in the interacting microfibrillar network is still proceeding. This means that fibrillation is controlled by the "chord

length distribution" of the tie molecules. As can be seen in the off-meridional sections (cf. Figure 4), even the reflections belonging to the four-point pattern show two maxima ($L_{1,om}$ and $L_{2,om}$), and moreover, $L_{2,om}$ is equal to the long period, L_{om}^{rel}, which is observed during relaxation of the interacting microfibrillar network as a whole. This finding shows that fibrillation does not specifically loosen the interconnections around single microfibrils but also those around thicker bundles of interconnected microfibrils, which are identified by the observation that they do not participate in the deformation cycles anymore.

In the next deformation interval ($\epsilon = 100-130\%$) even the average long period of the remnant microfibrillar network is decreasing, which means that now fibrillation is predominantly controlled by a limiting maximum long period of the microfibrillar network. At the end of this deformation interval, the fiber is completely fibrillated on the scale of the microfibrils and we only observe the layer-line pattern of noninteracting microfibrils.

During the last deformation interval for $\epsilon > 130\%$, the shape of the layer-line pattern hardly changes. The observed decrease of the intensity can be explained if we consider that in the fibrillated bristle at any external deformation only a few active microfibrils carry the load. When a microfibril becomes active, it is immediately elongated beyond its limit and thus its hard domains are destroyed.

Let us now consider the diffraction patterns of the relaxed sample (Figure 3b) and the corresponding morphological transitions. The first deformation interval [$\epsilon_r = 0-10(48)\%$] shows two-point layer-line patterns from an ensemble of relaxed microfibrils without interaction. The long spacing is constant at a value (L_1^{rel}, cf. Figure 4) very close to the initial long period of the predrawn bristle.

In the second deformation interval [$\epsilon_r = 10(48)-26(80)\%$] the layer-line pattern transits to a four-point pattern and the long period in the four-point pattern grows with increasing deformation. The analysis of the sections (Figure 4) yields that this transit is continuous. Again, as in the stressed state, this finding indicates the beginning of interaction among the microfibrils.

In the next higher deformation interval [$\epsilon_r = 26(80)-34(98)\%$] the four-point pattern is dominating. Now the average long period of the residual layer-line pattern moves to even lower values. This indicates the beginning destruction of noninteracting microfibrils, starting with those from the ensemble, which exhibit the highest long spacing.

In the fourth and in the fifth deformation interval [$\epsilon_r > 34(98)$] the intensity of the four-point maxima decreases and the pattern turns into a low-intensity two-point one. This finding strongly supports the notion of a fibrillation process, as explained in the discussion of the patterns from the stressed state. So in this deformation region microfibrils from the interacting microfibrillar network are isolated, while at the same time the isolated microfibrils are destroyed one by one.

In conclusion a substantial feature of these measurements must be emphasized. In addition to the observation of a six-point pattern and to the determination of the transverse long spacing, a very short measuring time of 2 min, in contrast to the previous investigations,[3,9] almost immediately after the removal of the external stress was used in the present work. The results show that the described changes in the conformation of the macromolecules in the amorphous regions (coiling and stretching), the relaxation of microfibrils due to the pulling out effect as well as the reversible morphological changes take less than 2 min, although the observable macroscopic shrinking of the bristle takes ca. 10 min.

Let us now go back to the results of the WAXS and specifically to Figure 8. It is well-known that the higher the FWHH, the lower the perfection of the crystallites. This means, in our case, that the perfection of the crystallites decreases with the rise of the overall deformation up to 100% and does not change with the further rise of the overall deformation up to 184% (Figure 8a). This effect, although not so well expressed, may be seen also in the case of relaxed sample, where the perfection of the crystallites decreases with the rise of the residual deformation up to $\epsilon_r = 34(98)\%$ and does not change with its further rise up to $\epsilon_r = 95(184)\%$ (Figure 8b). It seems almost obvious that pulling of hard segments out of the crystallites takes place with the progress of deformation, thus lowering their perfection. But considering Figure 8, there appear to be reversible and irreversible components in the changes of perfection of the crystallites. Presumably, the reversible part is due to the deformation of crystallites while the sample is under stress. The destruction of crystallites by pull-out of tie molecules appears to be the reason for the irreversible change. At deformation higher than 100%, the process of pulling out is almost completed and another phenomenon, namely slippage of microfibrils due to the stretching, occurs. The perfection of the crystallites does not change any longer and FWHH remains constant, as seen in Figure 8a,b. Another possible mechanism, namely breaking of interfibrillar tie molecules, may be rejected, since in this case the perfection would not change with the progress of the deformation. Thus, the results from WAXS independently confirm the mechanism of deformation proposed in the SAXS section of this work, as well as earlier.[3,9]

Conclusions

Five deformation intervals, dependent on the deformation level, were revealed for the thermoplastic elastomer in question. Two-, four- and unique six-point small-angle patterns as well as the corresponding transitions are characteristic features of these intervals. The preoriented polymer bristle can be considered as a bunch of microfibrils, which scatter independently for low deformations. For higher deformations, these microfibrils correlate in the transverse direction and the interfibrillar distance was calculated in this case. Due to the powerful synchrotron radiation, the six-point SAXS diagram, suggested earlier, is clearly seen in the third deformation interval. The pull-out mechanism was proven by both SAXS and WAXS investigations. Small-angle patterns, characterizing the very process of relaxation, were obtained by drastically decreasing the exposure down to 2 min.

Acknowledgment. It is a pleasure to acknowledge the financial support provided by NATO through grants CRG 920985 and CN.NIG 951394 and by the Bulgarian Ministry of Science, Education and Technology under contract X-542. Z.D. appreciates the hospitality of the Max-Planck-Institut für Polymerforschung, Mainz, Germany, where the wide-angle X-ray measurements were carried out. The technical help of M. Bach for these measurements is gratefully acknowledged. D.S. ap-

preciates the hospitality of Institut für Technische und Makromolekulare Chemie der Universität Hamburg, Hamburg, Germany, where part of this work was carried out in the frame of the Program of Materials Science TEMPUS, Project No 07183/94. This study was performed mainly in the frame of the Partnership Contract between the University of Hamburg and Sofia University.

References and Notes

(1) Adams, R. K.; Hoeschele, G. K. Thermoplastic Polyester Elastomers. In *Thermoplastic Elastomers: a Comprehensive Review*; Legge, N. R., Holden, G., Schroeder, H. E., Eds.; Hanser Publishers: Munich, 1987; p 164.
(2) Schoeder, H.; Cella, R. Polyesters, Thermoplastic. In *Encyclopedia of Polymer Science and Engineering*; John Wiley & Sons: New York, 1988; Vol. 12.
(3) Fakirov, S.; Fakirov, C.; Fischer, E. W.; Stamm, M. *Polymer* **1991**, *32*, 1173.
(4) Apostolov, A. A.; Fakirov, S. *J. Macromol. Sci., Phys. Ed.* **1992**, *B31* (3), 329.
(5) Fakirov, S.; Fakirov, C.; Fischer, E. W.; Stamm, M.; Apostolov, A. A. *Colloid Polym. Sci.* **1993**, *271*, 811.
(6) Denchev, Z.; Stamm, M.; Fakirov, S. Unpublished data.
(7) Fakirov, S.; Denchev, Z.; Apostolov, A. A.; Stamm, M.; Fakirov, C. *Colloid Polym. Sci.* **1994**, *272*, 1363.
(8) Gogeva, T.; Stankov, S.; Fakirov, S. *Commun. Dept. Chem. Bulg. Acad. Sci.* **1990**, *23*, 377.
(9) Fakirov, S.; Fakirov, C.; Fischer, E. W.; Stamm, M. *Polymer* **1992**, *33*, 3818.
(10) Fakirov, S.; Gogeva, T. *Macromol. Chem.* **1990**, *191*, 603.
(11) Fronk, W.; Wilke, W. *Colloid Polym. Sci.* **1985**, *263*, 97.
(12) Stribeck, N.; Sapoundjieva, D.; Apostolov, A. A.; Fakirov, S.; Zachmann, H. G. Europhysics Conference on Macromolecular Science: Application of Synchrotron Radiation in Polymer Science, Hamburg, Germany, September 13−15, 1995.
(13) Peterlin, A. *Text. Res. J.* **1972**, *42*, 20.
(14) Bonart, R. *Colloid Polym. Sci.* **1966**, *251*, 14.
(15) Balta-Calleja, F. J.; Vonk, C. G. *X-Ray Scattering of Synthetic Polymers*; Elsevier: Amsterdam, 1989; p 297.
(16) Pakula, T.; Saijo, K.; Hashimoto, T. *Macromolecules* **1985**, *18*, 1294.
(17) Blöchl, G.; Owen, A. J. *Colloid Polym. Sci.* **1984**, *262*, 793.
(18) Gerasimov, V. I.; Genin, Ya. V.; Kitaigorodsky, A. I.; Tsvankin, D. Ya. *Colloid Polym. Sci.* **1972**, *250*, 518.
(19) Fronk, W.; Wilke, W. *Colloid Polym. Sci.* **1983**, *261*, 1010.
(20) Sakurai, K.; Shikata, T.; Takahashi, T.; Matsuo, T.; Sakamaki, T.; Takahashi, S. *J. Macromol. Sci. Phys.* **1992**, *31*, 37.
(21) Bai, S. J.; Price, G. E. *Polymer* **1992**, *33*, 2136.
(22) Kumar, S.; Warner, S.; Grubb, D. T.; Adams, W. W. *Polymer* **1994**, *35*, 5408.

MA9612079